6. G. A. Filippov, E. V. Stekol'shchikov, and M. P. Anisimova, Teploénergatika, No. 3, 41-45 (1968).
7. A. L. Dushkin and A. I. Kolomentsev, in: Operating Process in Elements of Motors and Power Units with Two-Phase Working Medium [in Russian], Moscow (1980), pp. 8-15.
8. V. V. Fisenko, At. Tekh. Rubezh., No. 5, 41-47 (1977).
9. B. G. Pokusaev, in: Hydrodynamics and Heat Transfer in Two-Phase Media [in Russian], Novosibirsk (1981), pp. 81-90.
10. V. V. Fisenko et al., Izv. Vyssh. Uchebn. Zaved., Énerg., No. 1, 73-77 (1987).
11. H. Uchida and H. Nariai, in: Proceedings of Third Heat Transfer Conference, Vol. 5, Chicago (1966), pp. 1-12.

AERODYNAMICS OF A CIRCULATING FLUIDIZED BED

V. K. Maskaev, A. P. Baskakov,
A. G. Usol'tsev, and I. V. Ivanov

UDC 621.1:66.02

The authors present results of an experimental determination of the aerodynamic drag, density, velocity and dwell time of disperse material in a circulating bed.

It is known [1] that the region of stable pneumatic transport is determined by the speeds of the transporting gas, on the order of 10-15 m/sec. According to the data of [2], a reduction of the gas speed leads to increased slip velocity of the solid particles, accompanied by strong mixing of the material throughout the volume, predominantly ascending motion in the center of the channel, and sporadic slipping down motion along the walls.

The special features of the motion and distribution of the disperse material in the circulating bed, in comparison with pneumatic transportation, were studied on the extended experimental facility shown schematically in Fig. 1.

The facility consists of a channel 1 of internal diameter 250 mm, composed of 10 sections of length 950 mm each. The side surfaces of the sections had transparent windows for visual observation. The lowest section had a gas distribution grid 2 and performed the function of an aero chamber 3. The disperse material was supplied to the aero chamber from the storage bunker 4 via one of five interchangeable cantilevered screw-conveyer units 5, of internal diameter from 42 to 144 mm and volume rate up to 16.5 m^3/hr. The feed drive was actuated by the motor 6 through a transmission 7 and a safety device 8. The air was supplied from the air blower 9 through one of six standard diaphragms 10-15, and its pressure was regulated by the dump slide-valve 16. At the exit from the experimental channel the gas plus suspension reached the cyclone 17 of the first stage of cleaning. The trapped disperse material was collected in the bunker 18, and passing successively through valves 19 and 20, was routed as need be into the charging bunker 21 or for unloading via the hatch 22 into the box 23. The semi-clean gas was directed via the blower 24 to the cyclones 25 of the second stage of cleaning. The solid particles from the last cyclones were poured into the bunker 26 and unloaded through the hatch 27 and the box 28. The dust-free gas went to the ventilation box 29. In case more cleaning was needed the semi-clean gas was directed by the blower 30 to the bag filter 31, whence it went to the ventilation box 32. The disperse material was returned via valve 33 to the charge bunker. The hopper 34 was used to load fresh material. The operation of all the valves was actuated by the drive 35 from the motor 36. The gases were pumped out by the fan 37.

In the tests as the finely dispersed material we used aluminum hydroxide with a mean-mass diameter of 49 μ, as per GOST 118441-76, from the Polevskyi factory, for which the fractional composition is as follows:

S. M. Kirov Ural Polytechnic Institute, Sverdlovsk. Translated from Inzhenerno-Fizicheskii Zhurnal, Vol. 57, No. 5, November, 1989. Original article submitted April 5, 1988.

 0022-0841/89/5705-1312$12.50

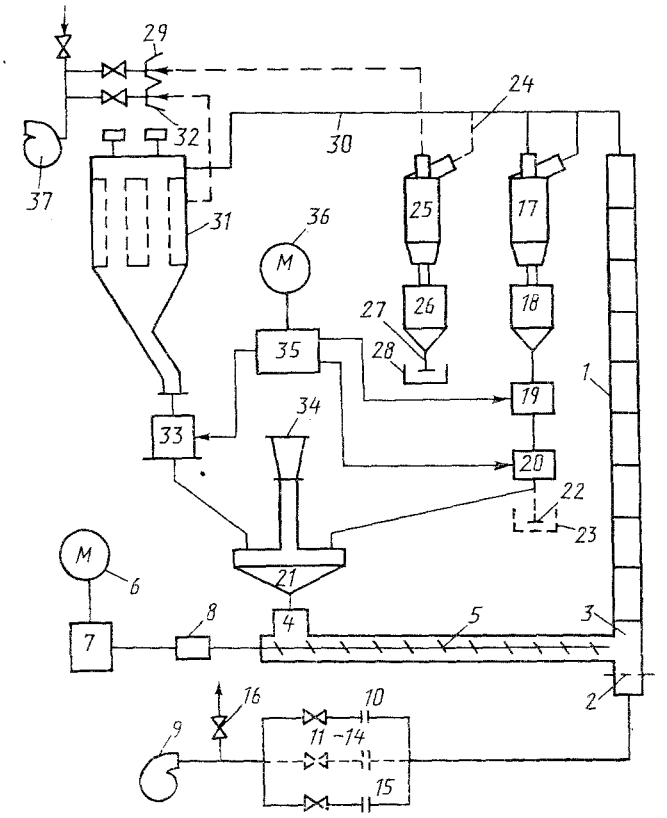

Fig. 1. Schematic of the experimental equipment.

Particle size, μ	Mass fraction, %
100—70	21,1
70—40	34,2
40—30	12,1
30—20	12,8
20—10	8,9
10—5	4,3
5—3	1,3
<3	5,3

The material had a fill density and a true density of 1349 and 2424 kg/m^3, respectively, and a feed rate of 0.4 m/sec for the coarsest fraction (85 μm), and 0.15 m/sec for the average.

The velocity of the fluidizing air varied from 2 to 22 m/sec, and its inlet temperature was kept in the range 30-40°C. The supply of disperse material could be varied in steps from 0 to 23.1 ton/hr, which corresponded to a variation of specific charge of material G_s as computed per 1 m^2 area of cross section of channel of up to 130.5 kg/m^2·sec. During charging the axis of the conveyer screw was located at a height of 175 mm from the level of the gas distribution grid, which had an aperture of diameter 2 mm and an active cross section of 10.2%.

During the investigation we tracked visually the behavior of the disperse system in the channel, and measured the aerodynamic resistance Δp relative to the top point, located at a height of 9.225 m from the level of the gas distribution grid, using 18 differential U-tube manometers. The static pressure was measured via 19 taps, the first of which was located at a height of 44 mm. The taps were connected to glass dust-settling chambers, to eliminate clogging up of the pressure-measurement tubes. In measuring the mean pressure drop values we smoothed the fluctuations by switching the common point to a damping chamber of volume 0.05 m^3.

As visual observations showed, when the gas filtration velocity w exceeded 8-9 m/sec, the particles moved upwards over the entire channel cross section, at all levels, and the pressure fluctuations practically vanished. For lower w and all material supply rates the pressure fluctuations increased, and for velocity w ≈ 3—6 m/sec and less the bed was clearly

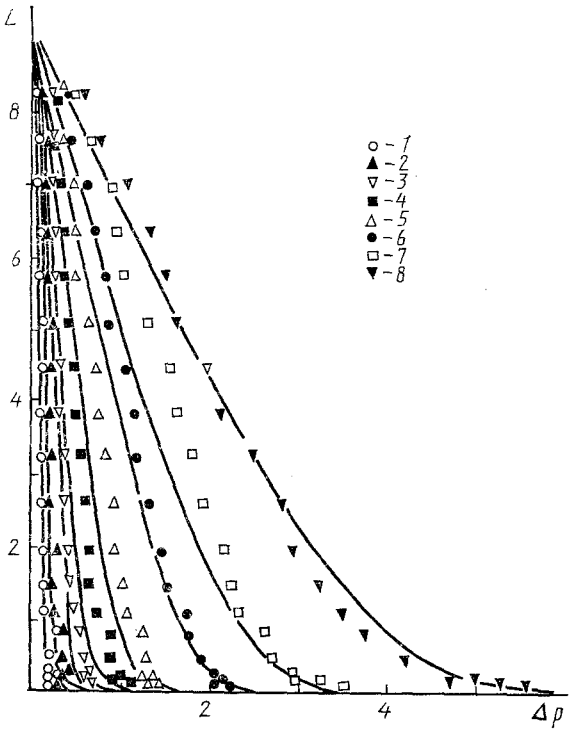

Fig. 2. Pressure distribution with height in the bed for a filtration speed w = 6.3 m/s (curves are computed from Eq. (11)): 1) G_S = 5.1 kg/(m²·sec); β = 0.8 kg/m³; 2) 8.7 and 1.4; 3) 14.1 and 2.2; 4) 20.4 and 3.2; 5) 33.1 and 5.2; 6) 55.1 and 8.8; 7) 78.3 and 12.6; 8) 130.5 and 21.1, Δp, kN/m²; L, m. The value of Δp is in kN/m², and L is in m.

divided into a central zone in which the disperse material was transported upwards by the gas, and a peripheral zone where it was predominantly driven along the walls in the form of jets and vortices, sometimes pouring down as a continuous stream to the center of the channel, periodically disrupted by the gas. The dropping motion of the particles along the walls increased very strongly with decrease of gas velocity, right down to 2 m/sec. Below this velocity no steady regime was obtained, since the resistance increased continuously, which led to deposition of the material, i.e., clogging up.

By way of illustration Fig. 2 shows results obtained with w = 6.3 m/sec and various values of β. For all the investigations of the β parameter the pressure varied with height of the upper part of the channel according to a law close to linear, while it increased sharply in the lower part of the bed for large β. In reducing the test data the channel was divided into three sections: a disperse material inlet section L_{1-4} of length 0.373 m with a maximum pressure gradient between points 1 and 4, distant 0.044 and 0.417 m, respectively, from the grid; a mean section L_{4-7} of length 1.062 m with an average pressure gradient between tap points 4 and 7, the last of which was located at height 1.479 m; and an established motion section L_{7-19} of length 7.746 m with the least pressure gradient between points 7 and 19.

Estimates show that the resistance in the motion of the gas-suspension in the channel in the range of concentration of disperse material and gas velocity investigated is due to practically the hydrostatic pressure of the bed of particles alone, since the fraction of the resistance due to friction of the particles and the gas on the channel walls does not exceed one percent, and the energy expended in accelerating the particles does not exceed 10% at velocities w of the order of 15-20 m/sec. The sum of the last two resistances does not exceed the experimental error, and we can neglect them. Thus, the bed density of disperse material in the channel can be determined from the formula

$$\rho = \frac{1}{g}\left(\frac{dp}{dl}\right) \simeq \frac{1}{g}$$

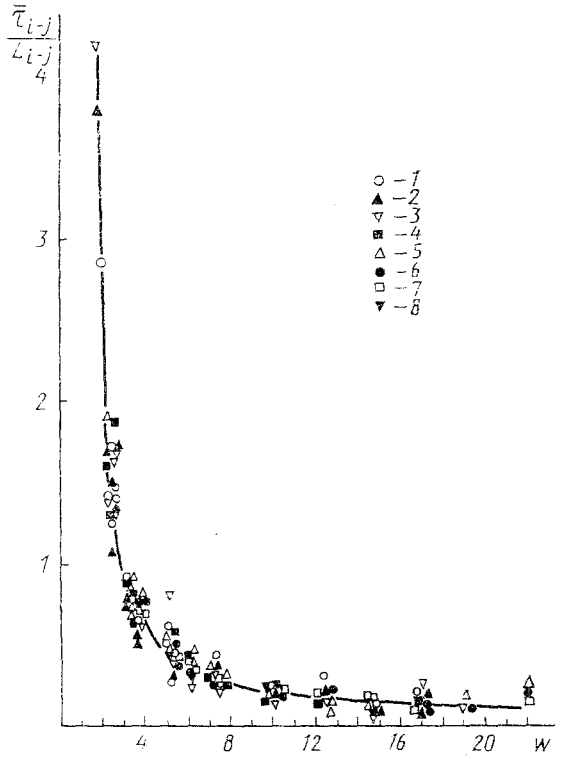

Fig. 3. Mean specific dwell time of the disperse material in the upper channel section as a function of the gas filtration rate (the points mean the same as in Fig. 2).

The mass of material in a section of length L_{i-j} is

$$M_{i-j} = \bar{\rho}_{i-j} S L_{i-j} = \rho_{i-j} S \bar{v}_{i-j} \bar{\tau}_{i-j}. \tag{2}$$

On the other hand, in the steady regime of operation of the facility we have

$$\bar{\tau}_{i-j} = \frac{M_{i-j}}{G_T} = \frac{L_{i-j}\bar{\rho}_{i-j}}{G_s}, \tag{3}$$

and the mean velocity of ascending motion of the particles is

$$\bar{v}_{i-j} = \frac{G_s}{\bar{\rho}_{i-j}}. \tag{4}$$

Figure 3 shows the mean dwell time $\bar{\tau}_{7-19}$ of (the motion of) the disperse material in the top section of the channel, divided by the length L_{7-19} of this section, i.e., more simply put, the mean dwell time in a section of the tube of length 1 m. As can be seen from Fig. 3, this quantity begins to increase markedly as the gas filtration velocity falls below 7-8 m/sec, and increases sharply for w ≈ 2–2.5 m/sec. The increase of dwell time is associated with the reduced speed of motion of the particles and results from the observed reverse motion, whose intensity increases with decrease of w. The dependences of $\bar{\tau}_{i-j}$ on w for the remaining bed sections are analogous.

Figure 4 shows the mean velocity of ascent of particles $\bar{v}_{i-j}$, computed from Eqs. (4) and (1), represented as a function of w. The variation of the mean velocity in the sections for all the values of G_S investigated is approximated satisfactorily by the relation

$$\bar{v}_{i-j} = a_{i-j} (\ln w)^{2.1}, \tag{5}$$

where a_{1-4} = 0.13; a_{4-7} = 0.4; a_{7-19} = 0.8; a_{1-19} = 0.6 m/s, and w is in m/s.

A comparison of the factors a_{i-j} shows that, in spite of the lengths of sections 1-4 and 4-7 differing by a factor of 3, the particle dwell time in each is almost the same. It is less than the dwell time in section 7-19 by a factor of 3.5, although the length of the latter is greater than that of the previous section by a factor of 7.5. Instead of Eq. (5) we can recommend a general dependence for any section length ℓ

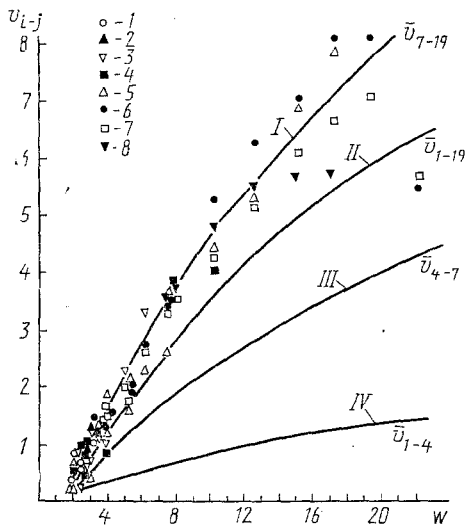

Fig. 4. The influence of gas filtration velocity on the mean particle speed in the channel (the point symbols are the same as in Fig. 2). The computation is per Eq. (5): I) with $a_{i-j} = 0.8$; II) 0.13; III) 0.4; IV) 0.6; $\bar{v}_{i-j}$; is in m/sec; w is in m/sec.

$$v(l,\ w) = \psi_l (\ln w)^{2,1}, \tag{6}$$

where

$$\psi_l = 0{,}43\, l^{0,6} - 0{,}02\, l^{1,6} \tag{7}$$

(ℓ is in m, and ψ_ℓ is in m/sec). The mean particle speed in the section $L_j - L_i$ is:

$$\bar{v}(L_i,\ L_j,\ w) = \frac{L_j - L_i}{\int_{L_i}^{L_j} \frac{dl}{\psi_l}} (\ln w)^{2,1}. \tag{8}$$

In the experiments we did not measure the bed resistance between the grid and the first point located at a height of 0.044 m from it. Since in calculations for equipment one must know the total bed resistance, we can estimate the resistance of this section by extrapolating Eq. (7) to some height $\ell = L_{min}$, less than 0.044 m, for the actual values of G_s, corresponding to the maximum possible density $L_{min} \ll 1$ of the saturated bed. Taking into account that we can neglect the second term in Eq. (7) for ρ_s, we have:

$$L_{min} = 4{,}1\, (G_s/\rho_s)^{1,67} (\ln w)^{-3,5}. \tag{9}$$

In practice we can compute the true bed density at height ℓ, its resistance and the mean dwell time of the disperse material from the formulas

$$\rho(l,\ w) = \frac{G_s}{\psi_l (\ln w)^{2,1}}, \tag{10}$$

$$\Delta p_L = g\rho_s L_{min} + \frac{gG_s}{(\ln w)^{2,1}} \int_{L_{min}}^{L} \frac{dl}{\psi_l}, \tag{11}$$

$$\tau_L = \frac{\Delta p_L}{gG_s}. \tag{12}$$

Approximating with Eq. (11) to the primary data of Fig. 2 we find satisfactory agreement with experiment. Equation (5)-(12) can be recommended for practical calculations of the basic parameters of a circulating fluidized bed.

NOTATION

ℓ, L, ambient and fixed bed height, m; v, velocity of a particle of disperse material, m/sec; w, velocity of the filtration gas, calculated on the empty channel section, m/sec; M,

mass of the disperse material, kg; GT, mass flow rate of disperse material, kg/s; S, cross section of the channel, m^2; $G_S = G_T/S$, specific load of disperse material, $kg/(m^2 \cdot sec)$; p, pressure, N/m^2; g, acceleration due to gravity, m/sec^2; $\beta = G_S/w$, dustiness of the gas, kg/m^3; ρ_S, saturation density of the bed of disperse material, kg/m^3; ρ, density of the fluidized bed, kg/m^3; τ, dwell time of the disperse material in the bed, sec. Subscripts: i, j, number of points; bar above – mean value.

LITERATURE CITED

1. I. M. Razumov, Pneumatic and Hydro-Transport in the Chemical Industry [in Russian], Moscow (1979).
2. J. Yerushalmi, D. H. Turner, and M. Squires, Ind. Eng. Chem., Processes Des. Dev., Vol. 15, No. 1, 47-53 (1976).

EXTERNAL HEAT TRANSFER IN AN ELECTRODYNAMICALLY FLUIDIZED BED

M. K. Bologa, A. B. Berkov, and V. L. Solomyanchuk

UDC 541.182.3:537.212

Heat-transfer trends are considered for a granular bed fluidized by electrical forces in a controlled gas atmosphere or under high vacuum.

A granular material can be fluidized by various means: hydrodynamically with a gas or liquid or by vibration, etc., which can greatly accelerate heat and mass transfer at immersed surfaces and between components [1-4]; it is widely used in engineering. Particle electrification during fluidization is usually considered an adverse effect that tends to reduce the heat transfer [2] because of aggregation and reduced mobility, with the heat-transfer surfaces being obstructed by electrically bound particles. It is found [5, 6] that strong external electric fields are ineffective in influencing the hydromechanics and heat transfer in pneumatically fluidized insulating-granule beds. However, if the particles are conducting or semiconducting, they can agitated vigorously by Coulomb forces [7], i.e., one can provide an electrodynamically fluidized bed. Some trends in such fluidization [7, 8] indicate that it is promising for use with low energy input and fine control. The trends in heat transfer for a planar horizontal electrodynamically fluidized bed [8-10] indicate that the transfer can be accelerated by up to a factor 80 by comparison with a gas layer, and this also provides some evidence on the heat-transfer mechanism there.

We have examined the heat transfer in such a bed for fairly wide ranges in the particle and dispersion-medium characteristics in order to identify the mechanism and extend the measurements.

We used stationary transfer conditions for a homogeneous part of a planar bed (Fig. 1), which was located in a sealed chamber on a vacuum line; this enabled us to examine the transfer under high vacuum or in a medium isolated from the atmosphere having the required composition and pressure. The fluidization was produced in a horizontal model having height h = 10 mm (Fig. 1) with upper heat-supply and lower cooled electrodes separated by a transparent ring insulator (lucite). At the edge of the gap adjoining the insulator, there were convergent conical parts representing electrostatic seals, angle between them 5.4°, while the outer boundary was a circle 200 mm in diameter. Those seals localized the fluidization in the inner plane-parallel part and ensured electrical strength for the inner insulator surface.

The stationary state was established, with the heat losses balanced by an isothermal jacket (Fig. 1), where we determined the heat-transfer coefficient K through the fluidized

Applied Physics Institute, Moldavian Academy of Sciences, Kishinev.

Translated from Inzhenerno-Fizicheskii Zhurnal, Vol. 57, No. 5, pp. 767-774, November, 1989. Original article submitted May 11, 1988.